First-principles study of the infrared spectrum in liquid water from a systematically improved description of H-bond network

Jianhang Xu,[1] Mohan Chen,[2] Cui Zhang,[3] and Xifan Wu[1,4]
[1]*Department of Physics, Temple University, Philadelphia, Pennsylvania 19122, USA*
[2]*CAPT, HEDPS, College of Engineering, Peking University, Beijing 100871, China*
[3]*Institute of Physics, Chinese Academy of Sciences, Beijing 100190, China*
[4]*Institute for Computational Molecular Science, Temple University, Philadelphia, Pennsylvania 19122, USA*

(Received 19 February 2019; revised manuscript received 18 April 2019; published 14 May 2019)

An accurate *ab initio* theory of the H-bond structure of liquid water requires a high-level exchange correlation approximation from density functional theory. Based on the liquid structures modeled by *ab initio* molecular dynamics by using maximally localized Wannier functions as a basis, we study the infrared spectrum of water within the canonical ensemble. In particular, we employ both the Perdew-Burke-Ernzerhof (PBE) functional within the generalized gradient approximation (GGA) and the state-of-the-art meta-GGA level approximation provided by the strongly constrained and appropriately normed (SCAN) functional. We demonstrate that the SCAN functional improves not only the water structure but also the theoretical infrared spectrum of water. Our analyses show that the improvement in the stretching and bending bands can be mainly attributed to better descriptions of directional H bonding and the covalency at the inter- and intramolecular levels, respectively. On the other hand, better agreements in libration and hindered translation bands are due to the improved dynamics of the H-bond network enabled by a less structured liquid in the experimental direction. The spectrum predicted by SCAN shows much better agreement with experimental data than the conventionally widely adopted PBE functional at the GGA level.

DOI: 10.1103/PhysRevB.99.205123

I. INTRODUCTION

As one of the most important materials on earth, water has an enormous impact on life. The unique functionalities of water lie in its liquid structure as depicted by the H-bond network. In this nearly tetrahedral structure, water molecules on neighboring sites are attracted by highly directional H bonds, which constantly break and reform under thermal fluctuations at ambient conditions. Not surprisingly, the fundamental understanding of liquid water properties is at the center of scientific interests [1–5].

Advanced experimental methods, such as scattering [6,7] and spectroscopy [8] techniques, have been developed and applied to detect the nature of the H bond in water. In particular, infrared (IR) spectroscopy provides a unique probe in which both the molecular configuration and its dynamics dielectric response can be inferred from the measured spectra [9,10]. In the IR spectrum, four main spectral features have been identified in experiments. Located in the relatively higher frequency range, the stretching and bending bands can be traced back to molecular vibrations in water vapor, which are strongly modified due to the presence of the H-bond network in the condensed phase. On the other hand, the libration and hindered translational bands with lower frequencies originate from the collective motion of water molecules in the H-bond network. Therefore, such vibrations have no counterparts in a single molecule.

Ab initio molecular dynamics (AIMD) simulation provides an ideal theoretical framework to study the IR spectra in water from first principles [11]. In AIMD simulations, water structures can be modeled by AIMD trajectories at finite temperatures, in which the forces acting on nuclei are obtained by the electronic ground state determined by density functional theory (DFT) [12,13]. The direct calculation of the IR spectrum is allowed by the advent of the modern theory of polarization given by the Berry phase formulation for extended systems [14]. The detailed dynamics dipolar correlation and its dependence on the H-bond network were further revealed later [15]. The above were facilitated by a rigorous decomposition of the overall polarization onto the electric dipoles belonging to individual water molecules based on maximally localized Wannier functions (MLWFs) [16].

Despite the above progress, difficulties remain when the computed IR spectrum is compared with available experiments. It is recognized that the accuracy of the predicted water structure depends on the level of the adopted exchange-correlation functional in DFT. For simulations of water, the generalized gradient approximation (GGA) [17] is widely applied. However, the GGA functional significantly overestimates the H-bonding strength as well as the polarizability of water, which is evidenced by the large redshift ($\sim$200 cm^{-1}) [15,18] of the computed stretching band compared to the experimental data. The above deficiency is partially due to the inherited self-interaction error. As a result, one electron state applies a spurious electrostatic interaction to itself [19]. By mixing a fraction of exact exchange, recent simulations showed that the underestimated stretching band in IR spectra of water can be largely improved by the PBE0-based AIMD simulation [20]. However, the application of hybrid DFT-based AIMD demands significantly increased computational

cost. For this reason, the available AIMD trajectories were relatively short, and the statistics was limited. Moreover, all the conventional functional approximations at the GGA level lack the description of long-range van der Waals (vdW) interactions. The long-range vdW is the key physical factor behind the larger mass density of water than that of ice [21,22]. Even in the canonical (NVT) ensemble, where the density of water is fixed to the experimental value at ambient conditions, the vdW-inclusive AIMD simulation was found to have large effects on the water structure, which can be seen by the enhanced population of water molecules in the interstitial region [23,24]. It is accepted that the long-range vdW interaction has a relatively small effect on the directional H bonding. However, water molecules in the interstitial region are expected to be weakly bonded or nonbonded. So far, it is unclear whether or not the increased fluctuation of water molecules in the interstitial region will affect the overall IR spectra in a nontrivial way. Clearly, improved modeling of the water structure and its dynamics via the DFT approach is a prerequisite for answering the above questions.

To address the above issues, we compute the IR spectrum of water from systematically improved modeling of liquid water by the strongly constrained and appropriately normed (SCAN) [25] meta-GGA functional. The IR spectrum computed from the conventional PBE-GGA [17] AIMD trajectory is also presented here for comparison. By satisfying all 17 known exact constraints on the semilocal functional, the recently developed SCAN functional presented a greatly improved description of both covalency in a water cluster [26] and the H-bond network in liquid water and ice [22,27]. Consistently, our computed IR spectrum based on SCAN-AIMD shows a significant improvement over the entire spectral range compared to the spectrum generated from the conventional PBE-GGA functional. The red frequency shift and overestimated amplitude of the stretching band obtained with the PBE-GGA functional are largely corrected by the improved directional H-bonding strength. By using the MLWFs as a basis, the increased population of water molecules in the interstitial region is found to be anticorrelated, which partially contributes to the decreased spectral amplitude towards the measured IR spectrum. The better agreement of the bending band frequency can be mainly attributed to the improved description of the covalency of water molecules. On the other hand, the blueshift of the libration modes towards the experimental direction is correlated to the improved prediction of the dynamical property in water.

II. METHODS

We computed the IR spectra of liquid water based on trajectories from Car-Parrinello molecular dynamics [11] using the QUANTUM ESPRESSO package [28]. The PBE and SCAN exchange-correlation functionals were used. Norm-conserving pseudopotentials [29] were adopted with an energy cutoff of 85 Ry. All simulations were carried out in a periodically cubic box with side lengths of 23.57 bohrs (12.47 Å), and 64 D_2O molecules were included in the box. The time step was set to 2 a.u. (~0.048 fs), with electron mass being 100 a.u. The temperature was set to 330 K, and the Nosé-Hoover thermostat [30,31] was adopted with the canonical ensemble.

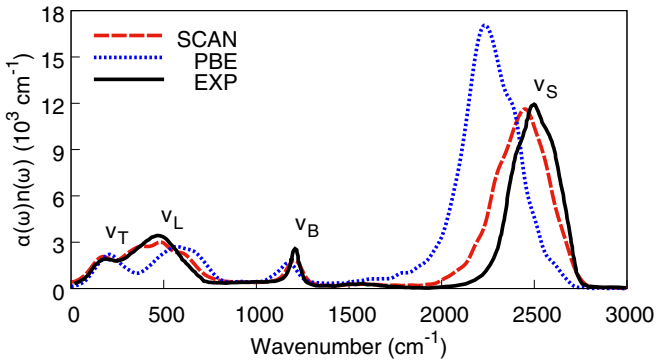

FIG. 1. IR spectra of liquid water obtained from AIMD simulations in the NVT ensembles. The experimental data are from Ref. [36] at room temperature. Labels ν_T, ν_L, ν_B, and ν_S correspond to translation, libration, DOD bending, and OD stretching peaks, respectively.

The 30 K increases to ambient temperature were applied to roughly mimic nuclear quantum effects on liquid structures, especially the oxygen-oxygen pair distribution function, and to be consistent with previous studies [22,32]. All simulations were run for more than 50 ps. In addition, we carried out ground-state DFT calculations for the water monomer in a cubic box with cell lengths of 30 bohrs (15.88 Å), using both SCAN and PBE with an energy cutoff of 250 Ry, to calculate the vibrational frequencies.

The IR spectra of liquid water are computed based on the IR absorption rate in terms of the total dipole moment. The formula [33] is derived using Fermi's golden rule and the Poynting vector with a classical approach [34] applied, where we treat the quantum time correlation function classically:

$$\alpha(\omega)n(\omega) = \frac{2\pi\beta\omega^2}{3cV}\int_{-\infty}^{+\infty} dt e^{-i\omega t}\langle M(0)M(t)\rangle, \qquad (1)$$

where $\alpha(\omega)$ is the light absorption coefficient per unit depth as a function of the frequency ω, $n(\omega)$ is the refractive index, and $\beta = (k_B T)^{-1}$, with k_B and T being the Boltzmann factor and temperature, respectively. The total dipole moment M in the simulation cell is computed via the formula $\sum_{i=1}^{n}\mu_i$, where the molecular dipole moment of the ith water molecule μ_i can be calculated via the position of nuclei and corresponding Wannier centers. Furthermore, we adopted a Gaussian window [35] in the form of $e^{-t^2/2\alpha^2}$ with $\alpha = 0.5$ ps when the discrete Fourier transform in Eq. (1) is performed.

III. RESULTS and DISCUSSION

As shown in Fig. 1, we present the theoretical IR spectra generated by SCAN-AIMD and PBE-AIMD trajectories. For comparison, the experimental spectrum is also shown. Four main dipole correlated vibrational bands can be identified in Fig. 1, whose characteristics belong to the hindered translation (T), libration (L), deuterium-oxygen-deuterium (DOD) bending (B), and the oxygen-deuterium (OD) stretching (S) modes with increasing frequencies. The IR spectrum computed from SCAN-AIMD shows a significantly improved accuracy comparable to that computed with the hybrid DFT functional [20], in which the better agreement with the

TABLE I. Water monomer (D_2O) vibration frequencies (in cm^{-1}). Subscripts *b*, *ss*, and *as* stand for bending, symmetric stretching, and antisymmetric stretching modes, respectively.

Method	ν_b	ν_{ss}	ν_{as}
SCAN	1193	2710	2832
PBE	1162	2660	2770
Expt. [37]	1206	2784	2889

experiment can be seen in both the spectral positions and spectral shape. The peaks of the above four bands, calculated by SCAN-AIMD, are centered at $\nu_T = 172$ (186) cm^{-1}, $\nu_L = 483$ (486) cm^{-1}, $\nu_B = 1207$ (1209) cm^{-1}, and $\nu_S = 2448$ (2498) cm^{-1}. In comparison, the same bands obtained from PBE-AIMD are predicted to be centered at $\nu_T = 207$ (186) cm^{-1}, $\nu_L = 572$ (486) cm^{-1}, $\nu_B = 1174$ (1209) cm^{-1}, and $\nu_S = 2233$ (2498) cm^{-1}, respectively. In the above, the values presented in the parentheses are taken from experiment [36]. In particular, the improvement by SCAN in the positions of the liberation and stretching modes is significant, which can be seen by the frequency shifts of ∼100 and ∼200 cm^{-1} respectively. At the same time, the spectral shape is also largely improved in the experimental direction, as clearly evidenced by the reduced intensity in the stretching band of more than 30%, which is severely overestimated at the PBE level.

The OD stretching band originates from the molecular vibrations in the water vapor (gas) phase. Based on the C_{2v} point group symmetry of the water monomer, these vibrations can be further categorized as symmetric and antisymmetric eigenmodes with a slightly higher frequency of the latter in experiments. Under the development of stretching modes, the covalent bond is elongated with a tendency towards dissociation, which also directly modifies the electric dipole of water molecules. Not surprisingly, the stretching band in the IR spectra not only locates at the highest-frequency range but also has the most prominent spectral intensity among the four IR spectral features. At the PBE level, the frequencies of both symmetric and antisymmetric modes in the gas phase are underestimated by more than ∼4% compared to experiment, as shown in Table I, which is consistent with the previous calculations [20]. Compared to PBE, the SCAN functional predicts better stretching frequencies in water's gas phase with an improvement of ∼2% towards experiment, as shown in Table I. The above can be attributed to the improved prediction of covalency in the water monomer. Indeed, the better agreement with experiments of the SCAN functional in terms of bond angle, bong length, and binding energies in a single water molecule and water clusters in the gas phase has been widely recognized recently [26,27].

In the liquid phase, the difference between symmetric and antisymmetric modes is smeared by the disordered environment, and the stretching band is formed. Moreover, the H bond, represented by the weak attraction of a proton to the oxygen lone pair of the neighboring molecules, also facilitates the elongation of OH bonds, as shown by the redshift of the stretching vibration by ∼300 cm^{-1} in liquid compared to the corresponding vibration in the vapor phase as measured

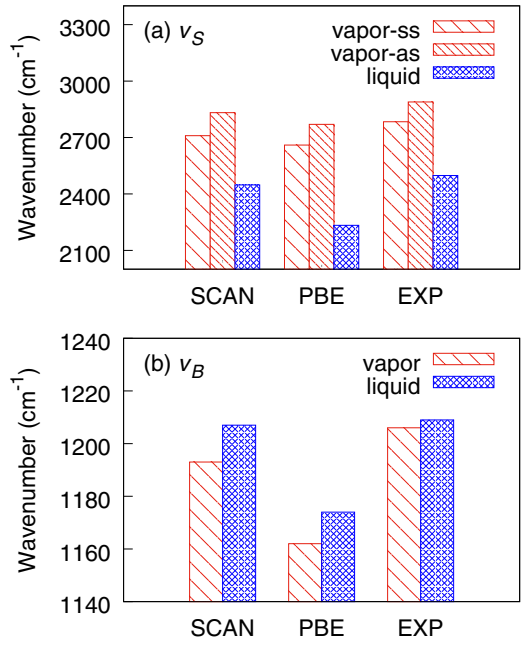

FIG. 2. (a) Stretching frequency ν_S and (b) bending frequency ν_B of a single water molecule (vapor) and liquid water compared using SCAN, PBE, and experiment data (EXP) for vapor [37] and liquid water [36]. (Note that the symmetric stretching frequency ν_{ss} and antisymmetric stretching frequency ν_{as} are listed separately for water vapor.)

experimentally in Fig. 2(a). However, due to the significant overestimation of the H-bond strength by the PBE functional, the stretching frequency of liquid water is predicted to be ∼500 cm^{-1} lower than that of water in the vapor phase. The H bond artificially strengthened by PBE also leads to the overestimated dipole-dipole correlation in the H-bond network, as evidenced by the much greater IR spectral intensity than the experimental spectrum in Fig. 1. In sharp contrast, the IR spectrum computed by the SCAN functional shows significantly better agreement in the above aspects. We attribute this improvement to the more accurate H-bond structure as well as the dynamical correlation described by the SCAN functional.

In order to elucidate the spectral signatures of liquid structure, we further decompose the overall spectrum into contributions from different ranges in the H-bond network. Based on the method introduced by Chen *et al.* [18], the total dipole correlation function in the temporal domain of Eq. (1) can be rewritten as the sum of a correlation function of any pair of water molecules as $\langle M(0)M(t)\rangle(r_1, r_2) = \langle\sum_{i,j}\mu_i(0)\mu_j(t)\rangle$. In the above, the electronic and ionic contributions of the dipole moment μ_i and μ_j of water molecules at any time t are rigorously determined by the Wannier centers and the ionic coordinates, respectively, both of which are generated on the fly in the AIMD simulation. Therefore, the spectrum can be divided into intramolecular IR_{self} $(i = j)$ and intermolecular $(i \neq j)$ parts [15]. In this work, we further divide the intermolecular part into spectral contributions from the first coordination shell IR_{1st}, water in the interstitial region $IR_{inters.}$, and water from the second shell and beyond $IR_{\geqslant 2nd}$ [38] based

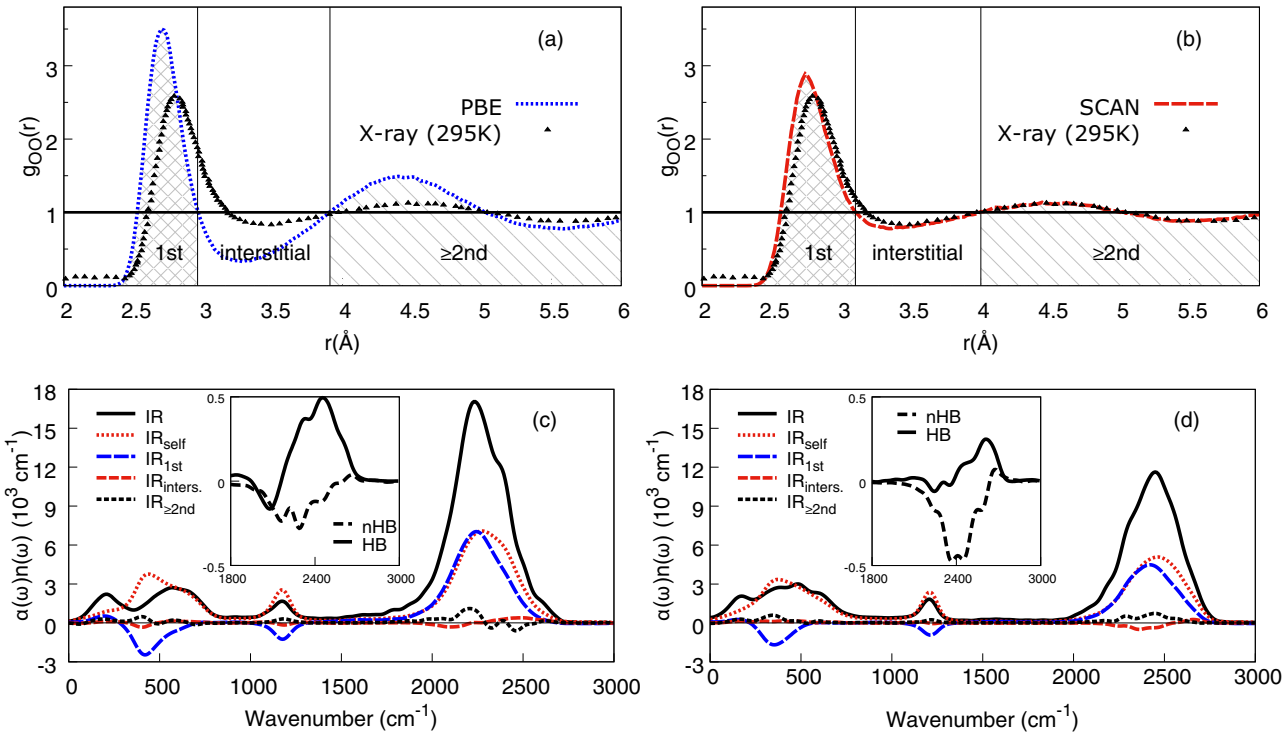

FIG. 3. Oxygen-oxygen pair distribution functions and the corresponding spatial decompositions by (a) PBE and (b) SCAN functionals compared with the x-ray diffraction experiment [7]. Intramolecular IR_{self} (red dotted lines) and spatial intermolecular IR_{1st}, $IR_{inters.}$, and $IR_{\geqslant 2nd}$ (colored dashed lines) contributions to the calculated IR spectra (black solid lines) using (c) PBE and (d) SCAN in the NVT ensemble. Decompositions of $IR_{inters.}$ into non-H-bonded (dashed lines) and H-bonded (solid lines) water contributions are shown in the insets in (c) and (d).

on the distance r_{ij} between the molecule pairs, as illustrated in Figs. 3(a) and 3(b). The criterion for the interstitial region is chosen to be 3.10 Å $\leqslant r_{ij} <$ 4.00 Å in SCAN and 2.96 Å $\leqslant r_{ij} <$ 3.91 Å in PBE, where the oxygen-oxygen pair distribution function $g_{OO}(r)$ is less than 1 between the first and second peaks. In the decomposition, water molecules are considered to be H bonded if the O-O distance is less than 3.5 Å and the OOD angle (the angle between O-O direction and O-D covalent bond direction) is less than 30° [39]. The resulting spectral decompositions and the corresponding $g_{OO}(r)$ are shown in Fig. 3 for both PBE and SCAN functionals.

Dynamically, the stretching mode not only modifies the electric dipole of the water molecule under vibration but also strongly polarizes the surrounding water molecules via the H bonds. Therefore, the stretching band of the IR spectrum is dominated by both the IR_{self} and IR_{1st} contributions. Such an effect has been well captured by both the SCAN and PBE functionals, which can be seen by the large and comparable intensities from these two decompositions. In the above, IR_{self} has a slightly higher frequency than that of IR_{1st}. This is not surprising since IR_{1st} is more sensitive to the H-bond network, while IR_{self} is instead more affected by the intrinsic vibration of the water monomer. However, the IR spectrum from the PBE functional suffers from clear drawbacks. Compared to the experimental measurement, $g_{OO}(r)$ is significantly overstructured, with a shorter first peak position than the experimental measurement, indicating the overestimated H-bond strength, as shown in Fig. 3(a). As a result, the stretching band of the IR spectrum computed at the PBE level is centered at a much lower frequency of 2233 cm^{-1} with a much higher intensity in comparison to experimental measurements. This is consistent with the fact that PBE predicts the proton is more delocalized and easier to donate to the neighboring water molecules than it should be. Such a severely overestimated directional H-bond strength is largely improved by the SCAN functional, which can be seen by the less structured coordination shell and increased distance of the first peak in $g_{OO}(r)$, as shown in Fig. 3(b). The softer H-bond network in the experimental direction also generates less polarizable liquid water, as indicated by the average electric dipole predicted by SCAN (2.95 ± 0.28 D) being much closer to the experimental reference (2.9 ± 0.6 D) [40] than that of PBE (3.22 ± 0.29 D). As expected, the stretching mode in the less polarizable medium becomes harder and shifts the stretching band center to a higher frequency at 2448 cm^{-1} and reduces intensities mainly from IR_{self} and IR_{1st}.

The dynamical polar correlation from the stretching vibration decays rather rapidly for water molecules separated by a distance farther away from the first coordination shell, which is qualitatively similar for both PBE and SCAN predictions, as shown in Figs. 3(c) and 3(d). Indeed, it is consistent with the weaker structural correlations in the radial distribution $g_{OO}(r)$ beyond the first peak in Figs. 3(a) and 3(b). However, the drawbacks can still be identified due to the overstructured liquid water by the PBE functional. On the one hand, the spectral contribution from water in the second shell and beyond $IR_{\geqslant 2nd}$ is predicted to have a higher

intensity in PBE than that from SCAN. On the other hand, due to the artificially strengthened H-bond strength, most water molecules in the interstitial region are still H bonded to the central molecule under stretching motion, giving rise to the positive spectral intensity in the inset of Fig. 3(c). However, the opposite trend is observed in the prediction by the SCAN functional, in which the water molecules in the interstitial region are mostly nonbounded with the observed anticorrelation, as seen by the negative spectral intensity in the inset of Fig. 3(d). It should be noted that the increasingly populated water molecules in the interstitial region should be attributed to the intermediate-range vdW interactions captured by the SCAN function, which is found to be the key physical effect in predicting a higher mass density of water than that of ice [22]. With the weaker dipole correlations from water molecules beyond the first coordination shell that are correctly predicted by the SCAN functional, the IR spectral intensity overestimated by PBE is further reduced in the experimental direction.

Moreover, a shoulder around $\sim$2300 cm^{-1} on the left-hand side of the peak is identified in the stretching band in experimental spectra of water. According to recent theoretical analyses [41,42], this shoulder feature is attributed to the so-called Fermi resonance which describes the spectral enhancement due to the intramolecular vibrational coupling between the OD stretching mode and the overtone of the bending mode. At both PBE and SCAN levels of studies, the shoulder appears roughly at the same position around 2300 cm^{-1}. This is not surprising since the bending overtone in this frequency range carries twice the frequency of water bending motion, and both PBE and SCAN yield a reasonably accurate bending frequency around 1200 cm^{-1}. Nevertheless, the relative position of the Fermi resonance shoulder feature is misplaced, which shows a blueshift appearing on the right-hand side of the stretching peak in the IR spectroscopy at the PBE level in Fig. 1.

In sharp contrast, as the SCAN functional accurately predicted the OD stretching frequencies, the shoulder emerges clearly, as shown in Fig. 1. At the same time, more pronounced enhancement of IR spectral amplitudes is observed for $\mathrm{IR}_{\mathrm{self}}$ and $\mathrm{IR}_{\mathrm{1st}}$ in the above frequency region for the spectrum by SCAN. The above is exactly consistent with the intramolecular vibrational coupling nature of the Fermi resonance [41,42].

Among the four spectral features, the bending band has the second-highest frequency centered at around 1200 cm^{-1}, which originates from the bending mode of the water monomer. Under the bending mode, the DOD bonding angle is modulated, which in turn changes the electric dipole of the molecule, but with a much weaker coupling strength than the stretching mode. Not surprisingly, the resulting spectral intensity is also smaller than the stretching band. In the vapor phase, the frequency of the bending mode is underestimated by $\sim$4% at the PBE level, while the calculation by the SCAN functional gives rise to a much more accurate value with an error of $\sim$1% compared to experiment at 1206 cm^{-1} in Table I and Fig. 2(b). Clearly, such a significant improvement should again be attributed to the better description of the covalency by SCAN. Indeed, the bonding angle and bonding length of the water monomer are respectively found to be 104.4° (104.5°) and 0.961 Å (0.957 Å) by SCAN, showing a large improvement over the PBE functional with values of 104.2° and 0.970 Å compared to the experimental values in the parentheses [26].

In the condensed phase, instead of discrete levels, the bending band is formed by the disordered liquid structure. According to the spectral decompositions in Figs. 3(c) and 3(d), the bending band is mainly contributed by the intramolecular contribution and the first coordination shell. In particular, the water molecules in the first coordination shell provide a large negative spectral intensity resulting from its anticorrelation nature. This is not surprising since the protons under the bending mode move along the normal direction of the H bond. Therefore, the development of the bending vibration needs to overcome the energy to break the H bond and generate out-of-phase dynamical dipole correlation [18]. As a result, unlike the stretch band, the presence of the H-bond network in liquid water impedes the bending mode, resulting in a slightly increased frequency relative to that in water vapor in experiment. Such a feature has been qualitatively predicted in both PBE and SCAN functionals. Clearly, the frequency difference is still overestimated by roughly the same magnitude for both functionals. The deficiency is likely due to the self-interaction error inherited in both GGA and meta-GGA functionals, resulting in the delocalized protons that are more easily donated to the neighboring oxygen atom.

In the far-infrared region in Fig. 1, the two spectral features in a rather broad distribution are associated with the collective vibrations on the H-bond network, which emerge in condensed phases such as ice and water. The feature at the higher-frequency branch around $\sim$500 cm^{-1} is attributed to the libration mode. Depicted by water libration, the water molecules undergo hindered rotational motions restricted by the presence of the H-bond network. Therefore, such a spectral signal is absent in water vapor since it is free to rotate an isolated molecule. Like the bending motion, water molecules under libration also need to overcome the energy barrier by breaking H bonds. Consistently, the spectral decomposition from intramolecular and first coordination contributions is dominant, in which the latter is characterized by the anticorrelation with negative spectral intensities, as shown in Figs. 3(c) and 3(d). Because of the overstructured H-bond network, the frequency of the libration motion is exaggerated $\sim$20% by the PBE functional, centered at 572 cm^{-1}. The less structured liquid water modeled by the SCAN functional eases the water libration at 483 cm^{-1}, matching accurately the experimental data at 486 cm^{-1}. Because the direction of water polarity aligns along the HOH angular bisector, the hindered water rotation is also highly associated with dynamical properties such as the rotational diffusion constant and rotational relaxation time which is accessible to experiments. The relaxation time τ_n is obtained by fitting with $e^{-t/\tau}$ to the nth-order rotational correlation functions, which are defined by the time correlation function $C_n(t) = \langle P_n[\hat{\boldsymbol{u}}(0)\hat{\boldsymbol{u}}(t)]\rangle$. Here P_n is the nth Legendre polynomial, and $\hat{\boldsymbol{u}}$ is the in-plane unit vector along the symmetry axis of a water molecule. To this end, we compute the first-order rotational correlation function $C_1(t)$ and the corresponding relaxation time τ_1 based on trajectories from both the PBE and SCAN functionals, as shown in Fig. 4. It should be noted that features at the beginning of the rotational correlation

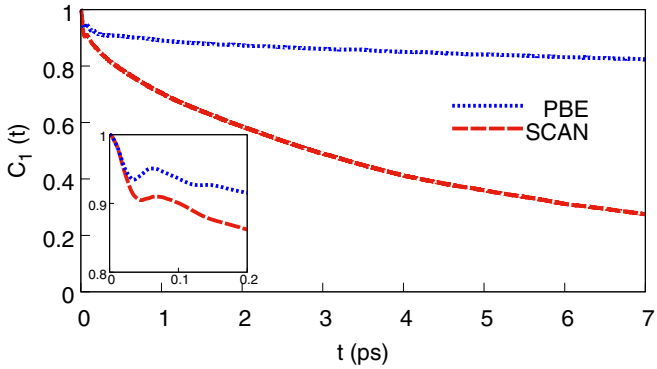

FIG. 4. First-order rotational correlation functions of liquid water obtained from AIMD simulations with SCAN (red dashed line) and PBE (blue dotted line) in the NVT ensembles. The inset shows enlarged rotational correlation functions in the first 0.2 ps.

function around 0.066 and 0.062 ps, magnified in the insets of Fig. 4, correspond to the libration motion that is observed in the frequency domain in Fig. 3. As time passes, the rotational correlation decays in both trajectories, giving rise to the relaxation time τ_1. Under Debye's model, the relation between relaxation time τ_n and the rotational diffusion constant D_R takes the form of $\tau_n = 1/[n(n+1)D_R]$. In the above, the rotational diffusion constant D_R is given by the inverse of τ_1, which is measured to be 2.0–7.5 ps [43]. Clearly, the overstructured water model by the PBE functional hampers the rotation motion and predicts an unphysically long relaxation time $\tau_1 = 20.91(\pm 0.22)$ ps with a corresponding small rotational diffusion constant $D_R = 0.047\,\mathrm{ps}^{-1}$. In sharp contrast, the less structured water modeled by the SCAN functional largely facilitates the water rotation and gives rise to much more reasonable values of $\tau_1 = 4.08(\pm 0.02)$ ps and $D_R = 0.24\,\mathrm{ps}^{-1}$. The result is consistent with previous studies on the diffusion coefficient [27]. In conclusion, the modified libration peak from the SCAN functional indicates an improved description of the diffusion-related dynamics in liquid water.

In the gas phase, the water molecule is free to undergo a translation motion in space. In liquid, water molecules, however, undergo hindered translation constrained by the H-bond network, which is depicted by the lower branch feature of the far-infrared band centered at $\sim$200 cm^{-1} in Fig. 1. Similar to the stretching mode, the spectral decomposition in Fig. 3 shows that the IR signals are mainly contributed by the dynamical correlation from the intramolecular contribution and molecules in the first coordination shell, which is consistent with the first-principles study of Chen *et al.* [18]. Unlike the stretching mode that is directly coupled to the electric dipole, the dynamical correlation here is generated by the induced dipole-dipole interaction under the hindered translation motion [44]. Therefore, the intensities of hindered translation are much weaker than those in the stretching band, as shown in Fig. 3. Not surprisingly, the artificially overstructured liquid water predicted by the PBE functional overestimates the energy barrier cost of hindered translation, which is evidenced by an overestimated peak position at 207 cm^{-1} compared to the experimental value of 186 cm^{-1}. On the other hand, the less structured liquid water model of the SCAN functional facilitates the water translation with a slightly underestimated value of 172 cm^{-1}.

It is well accepted that the liquid water structure under PBE prediction is icelike, which is not only overstructured but also sluggish and barely diffuses in space. As a result, the overall shape of the libration and hindered translation band is also icelike under the PBE prediction, as shown in Fig. 1. In the above, the distinction between the two modes is exaggerated by the rather deep minimum with a frequency gap around 370 cm^{-1}. Indeed, in the crystalline ice, the libration and hindered translation are two distinct spectral bands, which are separated completely with frequencies of 640 and 222 cm^{-1} in experiment [45], respectively. Strikingly, the above icelike error is mostly corrected in the spectrum modeled by the SCAN functional. For a liquid water structure that is more softened and disordered towards the experimental direction, the distinction between libration and hindered translation is also smeared, as shown in Fig. 1.

IV. CONCLUSION

In conclusion, we have performed a careful and comparative first-principles molecular dynamics study of the IR spectra of liquid water obtained by SCAN meta-GGA and PBE-GGA functionals. Our results showed the SCAN meta-GGA functional provides significant improvements for all four peaks in the IR spectra, compared to those obtained by PBE. Our analysis demonstrated that the SCAN functional models water more precisely on both the molecular and liquid levels and gives better descriptions of the electronic structure, range-dependent correlations, and dynamical properties. On the one hand, SCAN reaches the accuracy level of the IR spectra obtained by the PBE0 hybrid functional [20], with a relatively low computational cost. On the other hand, one may expect that the hybrid functional SCAN0 would mitigate the self-interaction error in DFT and would bring the calculated IR spectra closer to the experiments. Furthermore, recent studies [42,46,47] suggested that nuclear quantum effects due to light protons play a crucial role in obtaining accurate liquid water properties. The role played by quantum nuclei awaits future investigation, which is likely to broaden the spectral features and slightly reduce the frequencies of the stretching band due to the delocalized protons.

ACKNOWLEDGMENTS

This work was supported as part of the Center for the Computational Design of Functional Layered Materials, an Energy Frontier Research Center funded by the U.S. Department of Energy, Office of Science, Basic Energy Sciences, under Grant No. DE-SC0012575. X.W. is partially supported by the National Science Foundation through Grant No. DMR-1552287. The computational work used resources of the National Energy Research Scientific Computing Center (NERSC), a U.S. Department of Energy Office of Science User Facility operated under Contract No. DE-AC02-05CH11231.

[1] C. W. Swartz and X. Wu, Phys. Rev. Lett. **111**, 087801 (2013).
[2] M. Thämer, L. D. Marco, K. Ramasesha, A. Mandal, and A. Tokmakoff, Science **350**, 78 (2015).
[3] K. H. Kim, A. Späh, H. Pathak, F. Perakis, D. Mariedahl, K. Amann-Winkel, J. A. Sellberg, J. H. Lee, S. Kim, J. Park, K. H. Nam, T. Katayama, and A. Nilsson, Science **358**, 1589 (2017).
[4] P. G. Debenedetti and M. L. Klein, Proc. Natl. Acad. Sci. USA **114**, 13325 (2017).
[5] M. Chen, L. Zheng, B. Santra, H.-Y. Ko, R. A. DiStasio, Jr., M. L. Klein, R. Car, and X. Wu, Nat. Chem. **10**, 413 (2018).
[6] A. K. Soper, Int. Scholarly Res. Not. **2013**, 279463 (2013).
[7] L. B. Skinner, C. Huang, D. Schlesinger, L. G. M. Pettersson, A. Nilsson, and C. J. Benmore, J. Chem. Phys. **138**, 074506 (2013).
[8] T. Fransson, Y. Harada, N. Kosugi, N. A. Besley, B. Winter, J. J. Rehr, L. G. M. Pettersson, and A. Nilsson, Chem. Rev. **116**, 7551 (2016).
[9] J.-B. Brubach, A. Mermet, A. Filabozzi, A. Gerschel, and P. Roy, J. Chem. Phys. **122**, 184509 (2005).
[10] B. Auer, R. Kumar, J. R. Schmidt, and J. L. Skinner, Proc. Natl. Acad. Sci. USA **104**, 14215 (2007).
[11] R. Car and M. Parrinello, Phys. Rev. Lett. **55**, 2471 (1985).
[12] P. Hohenberg and W. Kohn, Phys. Rev. **136**, B864 (1964).
[13] W. Kohn and L. J. Sham, Phys. Rev. **140**, A1133 (1965).
[14] R. D. King-Smith and D. Vanderbilt, Phys. Rev. B **47**, 1651 (1993).
[15] M. Sharma, R. Resta, and R. Car, Phys. Rev. Lett. **95**, 187401 (2005).
[16] N. Marzari, A. A. Mostofi, J. R. Yates, I. Souza, and D. Vanderbilt, Rev. Mod. Phys. **84**, 1419 (2012).
[17] J. P. Perdew, K. Burke, and M. Ernzerhof, Phys. Rev. Lett. **77**, 3865 (1996).
[18] W. Chen, M. Sharma, R. Resta, G. Galli, and R. Car, Phys. Rev. B **77**, 245114 (2008).
[19] J. P. Perdew and A. Zunger, Phys. Rev. B **23**, 5048 (1981).
[20] C. Zhang, D. Donadio, F. Gygi, and G. Galli, J. Chem. Theory Comput. **7**, 1443 (2011).
[21] C. Zhang, J. Wu, G. Galli, and F. Gygi, J. Chem. Theory Comput. **7**, 3054 (2011).
[22] M. Chen, H.-Y. Ko, R. C. Remsing, M. F. Calegari Andrade, B. Santra, Z. Sun, A. Selloni, R. Car, M. L. Klein, J. P. Perdew, and X. Wu, Proc. Natl. Acad. Sci. USA **114**, 10846 (2017).
[23] J. Schmidt, J. VandeVondele, I.-F. W. Kuo, D. Sebastiani, J. I. Siepmann, J. Hutter, and C. J. Mundy, J. Phys. Chem. B **113**, 11959 (2009).
[24] J. Hermann, R. A. DiStasio, and A. Tkatchenko, Chem. Rev. **117**, 4714 (2017).
[25] J. Sun, A. Ruzsinszky, and J. P. Perdew, Phys. Rev. Lett. **115**, 036402 (2015).
[26] J. Sun, R. C. Remsing, Y. Zhang, Z. Sun, A. Ruzsinszky, H. Peng, Z. Yang, A. Paul, U. Waghmare, X. Wu, M. L. Klein, and J. P. Perdew, Nat. Chem. **8**, 831 (2016).
[27] L. Zheng, M. Chen, Z. Sun, H.-Y. Ko, B. Santra, P. Dhuvad, and X. Wu, J. Chem. Phys. **148**, 164505 (2018).
[28] P. Giannozzi, O. Andreussi, T. Brumme, O. Bunau, M. Buongiorno Nardelli, M. Calandra, R. Car, C. Cavazzoni, D. Ceresoli, M. Cococcioni, N. Colonna, I. Carnimeo, A. Dal Corso, S. de Gironcoli, P. Delugas, R. A. DiStasio, A. Ferretti, A. Floris, G. Fratesi, G. Fugallo, R. Gebauer, U. Gerstmann, F. Giustino, T. Gorni, J. Jia, M. Kawamura, H.-Y. Ko, A. Kokalj, E. Küçükbenli, M. Lazzeri, M. Marsili, N. Marzari, F. Mauri, N. L. Nguyen, H.-V. Nguyen, A. Otero-de-la Roza, L. Paulatto, S. Poncé, D. Rocca, R. Sabatini, B. Santra, M. Schlipf, A. P. Seitsonen, A. Smogunov, I. Timrov, T. Thonhauser, P. Umari, N. Vast, X. Wu, and S. Baroni, J. Phys.: Condens. Matter **29**, 465901 (2017).
[29] D. R. Hamann, Phys. Rev. B **88**, 085117 (2013).
[30] S. Nosé, J. Chem. Phys. **81**, 511 (1984).
[31] W. G. Hoover, Phys. Rev. A **31**, 1695 (1985).
[32] J. A. Morrone and R. Car, Phys. Rev. Lett. **101**, 017801 (2008).
[33] D. A. McQuarrie, *Statistical Mechanics* (University Science Books, Sausalito, CA, 2000).
[34] J. S. Bader and B. J. Berne, J. Chem. Phys. **100**, 8359 (1994).
[35] F. J. Harris, Proc. IEEE **66**, 51 (1978).
[36] J.-J. Max and C. Chapados, J. Chem. Phys. **131**, 184505 (2009).
[37] W. S. Benedict, N. Gailar, and E. K. Plyler, J. Chem. Phys. **24**, 1139 (1956).
[38] In order to sample the angular distribution uniformly while calculating the IR spectra of the second shell and beyond, we apply an upper limit of the correlated distance that is half of the box length.
[39] A. Luzar and D. Chandler, Nature (London) **379**, 55 (1996).
[40] Y. S. Badyal, M.-L. Saboungi, D. L. Price, S. D. Shastri, D. R. Haeffner, and A. K. Soper, J. Chem. Phys. **112**, 9206 (2000).
[41] A. A. Kananenka and J. L. Skinner, J. Chem. Phys. **148**, 244107 (2018).
[42] K. M. Hunter, F. A. Shakib, and F. Paesani, J. Phys. Chem. B **122**, 10754 (2018).
[43] D. Laage and J. T. Hynes, J. Phys. Chem. B **112**, 14230 (2008).
[44] B. Guillot, J. Chem. Phys. **95**, 1543 (1991).
[45] D. S. Eisenberg and W. Kauzmann, *The Structure and Properties of Water*, Oxford Classic Texts in the Physical Sciences (Clarendon, Oxford, 2005).
[46] M. Ceriotti, J. Cuny, M. Parrinello, and D. E. Manolopoulos, Proc. Natl. Acad. Sci. USA **110**, 15591 (2013).
[47] Z. Sun, L. Zheng, M. Chen, M. L. Klein, F. Paesani, and X. Wu, Phys. Rev. Lett. **121**, 137401 (2018).